Ring solids and supersolids in spherical shell-shaped dipolar Bose-Einstein condensates

J. Sánchez-Baena,[1,*] R. Bombín,[1,2] and J. Boronat[1]

[1]Departament de Física, Universitat Politècnica de Catalunya, Campus Nord B4-B5, 08034 Barcelona, Spain
[2]Institut des Sciences Moléculaires (ISM), Université de Bordeaux, 351 Cours de la Libération, 33405 Talence, France

(Received 15 December 2023; accepted 17 July 2024; published 29 July 2024)

We study the interplay between the anisotropy of the dipole-dipole interaction and confinement in a curved geometry by means of the extended Gross-Pitaevskii equation, which allows us to characterize the ground state of a dipolar Bose gas under the confinement of a bubble trapping potential. We do so in terms of the scattering length a and the number of particles. We observe the emergence of a wide variety of dipolar solids, consisting on arrangements of different number of droplets along a ring over the equator of the spherical shell confinement. We also show that the transition between the different phases of the system can be engineered by varying a, the number of particles or the radius of the trap, parameters, which can be experimentally tuned. Finally, we show the importance of working in microgravity conditions as gravity unstabilizes the observed dipolar solids.

DOI: 10.1103/PhysRevResearch.6.033116

I. INTRODUCTION

Since the realization of the first Bose-Einstein condensate (BEC) in 1995, the research on ultracold gases has been boosted by the achievement of a high control over them. This allows to explore not only a wide range of interaction strengths but also different geometries, ranging from one to three dimensions. In recent years, with the development of trapping techniques, it has been possible to achieve more exotic geometries with nontrivial topologiese.g., rings or curved surfaces (see Ref. [1] for a review on trapping techniques). These advances have motivated experiments both in zero-gravity conditions [2] and with a gravity compensation mechanism [3] where the gravitational sag is absent and the BEC can be engineered in the shell of a sphere [4] (see [5] for recent reviews on the topic). Previous studies include the characterization of BEC condensation and excitations [6,7], the topological superfluid phase transition [8,9], the BEC-BCS crossover [10], the gas to soliton transition [11], the study of vortices and collective excitations [12] and the application of matter-wave lensing techniques [13]. On a less fundamental approach, the possibility of engineering atom-based circuits has also been explored [14].

In the context of ultracold gases, the study of dipolar systems has revealed astonishing phenomena such as droplet formation and the emergence of supersolidity (see Ref. [15] for an experimental review). Supersolidity refers to a state of matter that simultaneously features spatial diagonal and off-diagonal long-range order [16–18]. In fact, dipolar systems emerge as an exceptional setup for studying the phenomena of supersolidity. This topic has been extensively studied [19–32] and experimentally confirmed [33–44]. Supersolid phases have been also predicted to occur in strictly two-dimensional geometries, where the transition to the normal state is of the Berezinskii-Kosterlitz-Thouless type [25,26,45,46]. Nonetheless, only a few studies have considered this phenomena on curved surfaces (see Refs. [47–54]).

Dipolar shell-shaped systems are expected to exhibit a richer phase diagram than contact BEC gases [5]. On one hand, the long ranged and anisotropic character of dipolar interaction is known to produce density modulated phases with important long-range correlations in free space. On the other hand, the curvature would make the ground state of the system very different to that of the free space, for example by frustrating the formation of stripes. In this sense, the interplay between anisotropy, long-range order, and topology in spherically symmetric traps can give rise to BEC states in which the spherical symmetry of the trap is spontaneously broken.

To give some insight into the previously mentioned phenomena, in the present paper we study a dipolar Bose gas confined on a spherical bubble trapping potential in the regime of parameters where supersolidity arises. The paper is organized as follows. In Sec. II, we illustrate the methodology that we employ. The main results of our paper are presented and discussed in Sec. III. Finally, in Sec. IV we summarize the main conclusions and discuss future perspectives.

II. THEORY

We consider a system of N magnetic dipolar atoms of mass m with all their magnetic moments μ aligned along the z axis. The system is confined in a bubble trap potential [55,56]

$$V_{\mathrm{trap}}(\mathbf{r}) = m\omega_0^2 r_0^2 \sqrt{\frac{[(r/r_0)^2 - \Delta/\epsilon]^2}{4} + (\Omega/\epsilon)^2}, \qquad (1)$$

*Contact author: juan.sanchez.baena@upc.edu

where ω_0 is the frequency of the bare harmonic trap, prior to radiofrequency (rf) dressing, and the parameters Δ and Ω are the detuning between the radiofrequency (rf) field and the different energy states employed to prepare the condensate, and the Rabi coupling between these states, respectively [4,56]. We have also introduced the relevant length and energy scales, r_0 and ϵ respectively, given by $r_0 = 12\pi a_{\rm dd}$ and $\epsilon = \hbar^2/(mr_0^2)$, where $a_{\rm dd} = \frac{C_{\rm dd} m}{12\pi\hbar^2}$ is the dipole length, with $C_{\rm dd} = \mu_0\mu^2$, μ_0 the Bohr magneton and μ the magnetic dipole moment of the atoms. For simplicity, and analogously to a previous study [56], we consider $\Delta = \Omega$.

In order to characterize the ground state of the system in a spherically symmetric trap we solve the three-dimensional extended Gross-Pitaevskii equation that reads

$$\mu\Psi(\mathbf{r}) = \left[-\frac{\hbar^2}{2m}\nabla^2 + V_{\rm trap}(\mathbf{r}) + g|\Psi(r)|^2 + \gamma_{\rm QF}|\Psi(\mathbf{r})|^3 + \int d\mathbf{r}' V_{\rm dd}(\mathbf{r}-\mathbf{r}')|\Psi(\mathbf{r}')|^2\right]\Psi(\mathbf{r}) , \tag{2}$$

with μ the chemical potential, $\Psi(\mathbf{r})$ the condensate wave function, which is normalized as $N = \int d\mathbf{r}|\Psi(\mathbf{r})|^2$, and $g = 4\pi\hbar^2 a_s/m$ the coupling constant with a_s the s-wave scattering length. The fourth term $\gamma_{\rm QF}|\Psi|^3$ is the LHY (Lee-Huang-Yang) correction [57–59], which introduces quantum fluctuations,

$$\gamma_{\rm QF}|\Psi|^3 = \frac{32g\sqrt{a_s^3}}{3\sqrt{\pi}} Q_5(\varepsilon_{\rm dd})|\Psi|^3, \tag{3}$$

with $\varepsilon_{\rm dd} = a_{\rm dd}/a_s$ and $Q_5(\varepsilon_{\rm dd}) = \frac{1}{2}\int_0^\pi d\alpha \sin\alpha[1 + \varepsilon_{\rm dd}(3\cos^2\alpha - 1)]^{5/2}$. For values $\varepsilon_{\rm dd} > 1$ the Q_5 function has a small imaginary part that is discarded. Finally, the last term in Eq. (2) accounts for the dipole-dipole interaction (DDI),

$$V_{\rm dd}(\mathbf{r}-\mathbf{r}') = \frac{C_{\rm dd}}{4\pi}\frac{1-3\cos^2\theta}{|\mathbf{r}-\mathbf{r}'|^3}, \tag{4}$$

where θ is the polar angle of the vector $\mathbf{r}-\mathbf{r}'$.

The use of the pseudopotential in Eq. (2) [that is, the term $g|\Psi(r)|^2 + \int d\mathbf{r}' V_{\rm dd}(\mathbf{r}-\mathbf{r}')|\Psi(\mathbf{r}')|^2$] is justified as long as the collisions between particles can be treated as three-dimensional processes. The system lays in the two-dimensional regime if the harmonic length $a_{\rm ho} = \sqrt{\hbar/(m\omega_0)}$, which is associated to the tightness of the confinement, is significantly smaller than any other length scales. However, in our calculations, we choose a trapping strength such that $a_{\rm ho} \gg a_s$. Therefore, all scattering processes can be considered three-dimensional and the pseudopotential of Eq. (2) can be applied. In the case of a tight confinement (thin shell limit), a pseudopotential that considers the effects of the geometry should be employed [60,61].

In the majority of this paper, we restrict ourselves to the zero gravity limit. However, the effect of a gravitational force can be accounted for by adding the following one-body potential [49] to Eq. (2):

$$V_g(\mathbf{r}) = mg(x\sin\theta_g + z\cos\theta_g) , \tag{5}$$

where θ_g is the angle between the z axis and the gravity direction. For ^{164}Dy atoms, the gravitational strength on the Earth corresponds to to $mg = 1.15\epsilon/r_0 = mg_{\rm E}$. In Sec. III D, we study the robustness of a dipolar solid ring under the effect of gravity.

III. RING SOLIDS AND SUPERSOLIDS

As a means to illustrate the system under study, we show in Fig. 1 the probability density of the dipolar BEC confined within the bubble trap under zero gravity for different values of the ratio $\varepsilon_{\rm dd} = a_{\rm dd}/a_s$. We have employed a trap with parameters $\Delta/\epsilon = 400$, $\omega_0 = 0.22\epsilon/\hbar$, which correspond to $\omega_0 = 2\pi \times 200$ Hz and a bubble trap with radius $R = r_0\sqrt{\Delta/\epsilon} = 5.2$ μm for ^{164}Dy atoms. These parameters are realistic for existing setups with nondipolar gases. From the figure, we can see that in the contact dominated regime ($\varepsilon_{\rm dd} \ll 1$), the dipolar gas fills up the spherical shell, yielding an apparently spherically symmetric density distribution, despite the anisotropy of the DDI. As seen in Fig. 1, and as reported in previous studies [48,49], the atoms of the BEC gas tend to populate the equator of the shell, even before reaching the dipole dominated regime, $\varepsilon_{\rm dd} > 1$. This magnetostriction is a consequence of the competition between the anisotropy of the dipole-dipole interaction (which energetically favors head-to-tail arrangements of dipoles) and the shell shape of the external confinement. Experimentally, ring-shaped condensates can be obtained by the use of toroidal traps [50,62–64], which can also be realized in experiments [65–67]. However, in the present case, as well as for cylindrically shaped traps [68], the ring structure arises from the interplay of the anisotropy of the DDI and the geometry of the confinement, instead of being fully imposed by the trap, as it is the case for toroidal traps, which are ring shaped. For the rest of our paper, we focus on the regime $\varepsilon_{\rm dd} > 1$ and the aforementioned value of the trapping strength.

In the dipolar dominated regime ($\epsilon_{\rm dd} > 1$), the anisotropy of the dipolar interaction can give rise to dipolar solids and supersolids, in analogy to the phenomenology that takes place in bulk-trapped dipolar BECs. Equation (2) can numerically be solved for different values of the scattering length a_s (and thus, $\epsilon_{\rm dd}$) and number of particles N to obtain the ground state of the system. As reported in similar papers [63,69,70], the energy minimization has to be carefully performed, sampling a wide variety of initial conditions, as many metastable states close to the ground state exist. We detail in the Appendix the numerical parameters of our simulations, as well as the initial conditions considered. Since superfluid structures may arise, we evaluate the Leggett's upper bound estimator for the superfluid fraction [71], which is computed from the ground-state density as

$$f_s = \left[\frac{1}{2\pi}\int_0^{2\pi}\frac{d\theta}{\rho(\theta)/\rho_0}\right]^{-1}, \tag{6}$$

where

$$\rho(\theta) = \int dzdr\, r|\Psi(r,\theta,z)|^2, \tag{7}$$

$$\rho_0 = \frac{1}{2\pi}\int_0^{2\pi}\rho(\theta)d\theta . \tag{8}$$

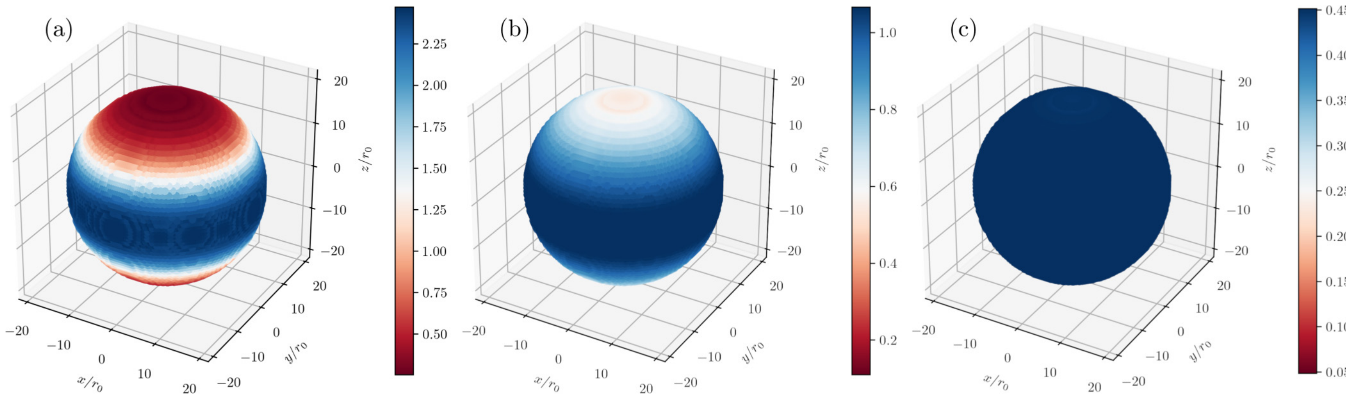

FIG. 1. Three-dimensional probability density of the dipolar BEC under a shell-shaped confinement [see Eq. (1)] with detuning $\Omega/\epsilon = \Delta/\epsilon = 400$ and bare harmonic frequency $\omega_0 = 0.22\epsilon/\hbar$. The probability density is reported at the surface $r = \sqrt{x^2+y^2+z^2} = r_0\sqrt{\Delta/\epsilon}$ for $\varepsilon_{dd} = 1.25$ (a), 0.5 (b), and 0.1 (c). The color bars indicate the value of $|\Psi(\mathbf{r})|^2$ in units of r_0^{-3}.

Equation (6) yields the trivial unity limit for a ring-like condensate [since $\rho(\theta)$ is a constant] and decreases as the modulation of the wave function increases along the ring. This upper bound estimator for the superfluidity has shown excellent agreement with the calculation of nonclassical translational inertia for a system of dipoles confined in a quasi-1D tubular geometry [31].

A. Structural diagram and transitions

The structural diagram of the system is reported in Fig. 2, where we show the two-dimensional integrated density $\rho(x, y) = \int dz|\Psi(\mathbf{r})|^2$ of each structure. Regarding the superfluid fraction along the ring, only the structures featuring dipolar clusters in the interval $\varepsilon_{dd} \in (1.36, 1.41)$ yield a significant superfluid fraction ($f_s > 0.2$), while for $\varepsilon_{dd} > 1.41$, the result of Eq. (6) quickly drops to zero. On the other hand, all the states in the SF region of Fig. 2 yield unit superfluidity. We label the states with $f_s = 1$ as superfluids, while we call supersolids and solids those, which yield $f_s > 0.2$ and $f_s < 0.2$, respectively. In general, the increase of ϵ_{dd} for a fixed number of particles implies a lower number of droplets, since the attraction of the DDI favors the bunching of dipoles and thus, fewer and more elongated clusters are formed. In much the same way, the decrease of the number of particles for a fixed ϵ_{dd} also causes a reduction in the number of droplets because the system wants to maximize the number of dipoles placed in a head-to-tail configuration. The peak density of the droplets that we obtain lies close to the expected values obtainable with harmonic traps (see the seminal experiment of Ref. [72]). For the largest number of particles ($N = 31500$) the peak density lies in the interval $\rho_{\text{peak}} \in [3, 100] \times 10^{14}\text{cm}^{-3}$, where the largest values are achieved for $\varepsilon_{dd} = 2$, for which all particles cluster into a single droplet. We also see that the solid structures disappear if the number of particles is decreased below a threshold, from which there is not enough density to sustain clustering. This phenomenology is reminiscent of a quasi-1D system of dipoles confined in a tube [30,31] where the disappearance of the supersolid phase in the low-density regime upon decreasing the density is also reported.

Precisely, in the spirit of these studies, it is interesting to examine the character (continuous or discontinuous) of the transition between the different structures present in the diagram of Fig. 2. We can not strictly speak of first- and second-order phase transitions (as it is done in [30,31]) because our system is finite. Our calculations show that the transition between different solid states is discontinuous, meaning that the system jumps from a state with a given number of droplets to a different one discontinuously (the density distribution changes abruptly). This is because there exists an energy crossing between the different metastable states at the transition boundary. We illustrate this in Fig. 3, where we report the energy difference between two dipolar solids across the transition between regions 3 and 4 of the diagram in Fig. 2 for $N = 31500$. In much the same way, the transition between a dipolar solid and the superfluid is also discontinuous for low enough density, in analogy to the first-order phase transition that takes place in the low-density regime of the tubular quasi-1D system. This is illustrated in Fig. 4, where we show the contrast of the BEC density across the transition between regions 2 and 7 of Fig. 2, for $N = 16500$. Here, the contrast is defined as

$$C = \frac{\rho_{\max} - \rho_{\min}}{\rho_{\max} + \rho_{\min}} \tag{9}$$

where $\rho_{\max}$ and $\rho_{\min}$ are, respectively, the maximum and minimum values of the integrated density $\rho(x, y)$ along the circle of radius $R/r_0 = \sqrt{\Delta/\epsilon}$. As one can see from Fig. 4, the contrast in the density shows a clear discontinuity. As one increases the density in the system, either by increasing the number of particles or by decreasing the available volume by tuning the trap, a continuous transition between the supersolid and fully superfluid states eventually takes place [63], as it happens in the quasi-1D geometry. We show in Fig. 5 an example of the continuous transition between a supersolid featuring 6 droplets and a superfluid ring, for which $N = 26500$. Therefore, in view of the results, we can draw similarities between the physics under our geometry and the quasi-1D tubular one, since the transitions that lead to a superfluid gas in our system are analogous to the first-order and second-order phase transitions of Refs. [30,31].

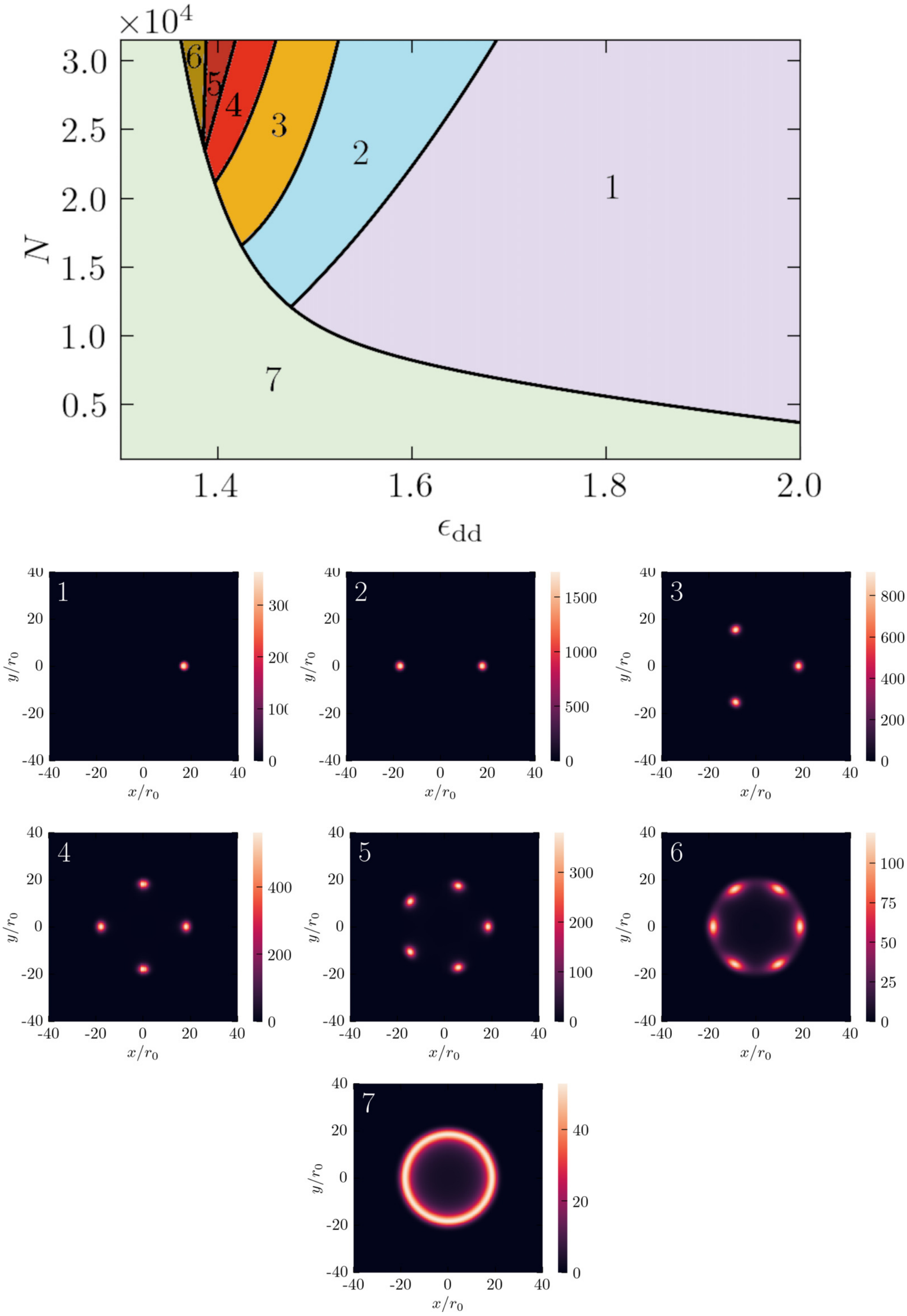

FIG. 2. (Top) Structural diagram of the ring-shaped dipolar condensate as a function of $\epsilon_{\rm dd} = a_{\rm dd}/a$ and the number of particles N. Panels 1–7: Integrated density profiles $\rho(x, y)$ of the condensate density arising in each region of the diagram. The color bars indicate the value of $\rho(x, y)$ in units of r_0^{-2}. The parameters for the bubble trap [see Eq. (1)] are $\Delta/\epsilon = \Omega/\epsilon = 400$, $\omega_0 = 0.22\epsilon/\hbar$.

B. Engineering supersolids

Even though the supersolid phase constitutes a small region in the diagram of Fig. 2 as mentioned previously, a rich variety of supersolid structures can be engineered when tuning Δ, and thus effectively modifying the radius of the trapping spherical shell. By increasing Δ starting from a conventional harmonically trap gas, the system transitions to a supersolid. Increasing further Δ leads to an increase in the number of droplets, all while retaining a substantial superfluid fraction and the ring shape. This is shown in Fig. 6, where we report the integrated density $\rho(x, y)$ of the condensate wave

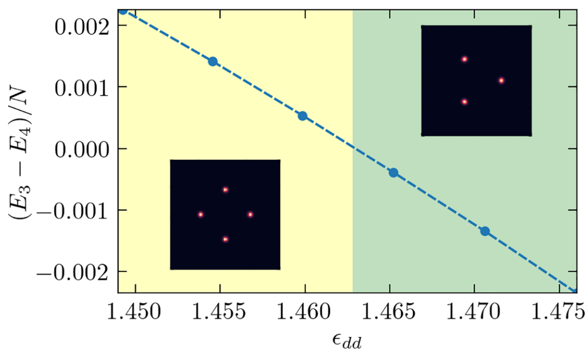

FIG. 3. Difference in the energy per particle between a solid state with three and four droplets as a function of $\varepsilon_{\rm dd}$ for $N = 31500$ and the same bubble trap as in Fig. 2.

function for different values of Δ. We also report Leggett's upper bound for the superfluid fraction [see Eq. (6)], which increases as the trap radius decreases, thus confirming that the superfluid density can be enhanced by reducing Δ. The variation of this parameter is pretty straightforward in experimental setups, as changing Δ is precisely how the bubble trap is generated from a harmonic potential. The wide variety of solid structures in the diagram of Fig. 2 thus allows for the observation of many different supersolid dipolar rings (i.e., supersolids with a different number of droplets) by playing with the parameter Δ starting from different points of the structural diagram. This is showcased in Fig. 7, where we show four examples of different supersolids obtained for different combinations of the number of particles, the detuning and the scattering length.

C. High particle number limit

Up to now, we have restricted the particle number to the interval $N \leqslant 31500$. However, it is interesting to consider higher particle numbers, specifically to check whether a new structure qualitatively different to the ones observed so far can emerge. In order to address this question, we have computed the ground state of the dipolar BEC for $N = 10^5$ and $N = 10^6$ for two different values of $\varepsilon_{\rm dd}$ ($\varepsilon_{\rm dd} = 1.42$ and $\varepsilon_{\rm dd} = 1.72$). For these cases, we show in Fig. 8 the integrated two-dimensional densities $\rho(x, y) = \int dz |\Psi(\mathbf{r})|^2$ and $\rho(x, z) = \int dy |\Psi(\mathbf{r})|^2$. As we can see from the figure, atoms accumulate on the central ring instead of forming

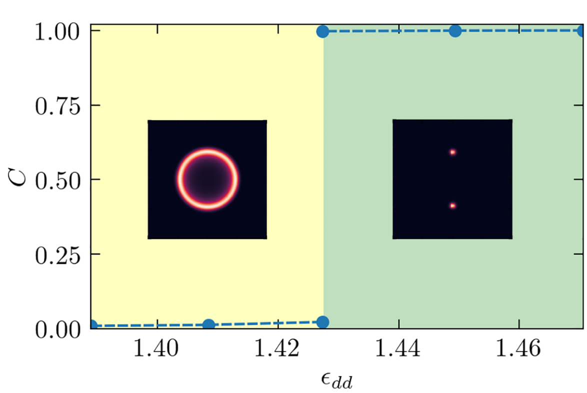

FIG. 4. Contrast of the BEC density [see Eq. (9)] as a function of $\varepsilon_{\rm dd}$ for $N = 16500$. The bubble trap parameters are the same as in Fig. 2.

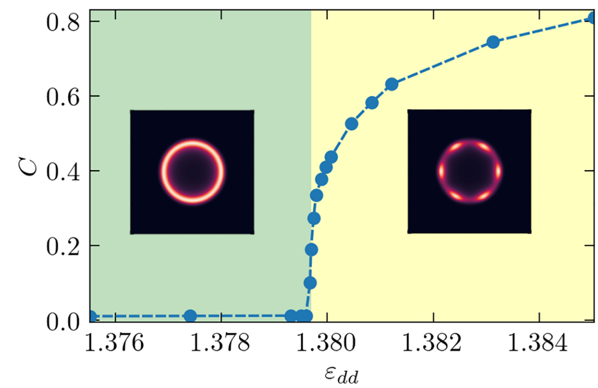

FIG. 5. Contrast of the BEC density [see Eq. (9)] as a function of $\varepsilon_{\rm dd}$ for $N = 26500$. The bubble trap parameters are the same as in Fig. 2.

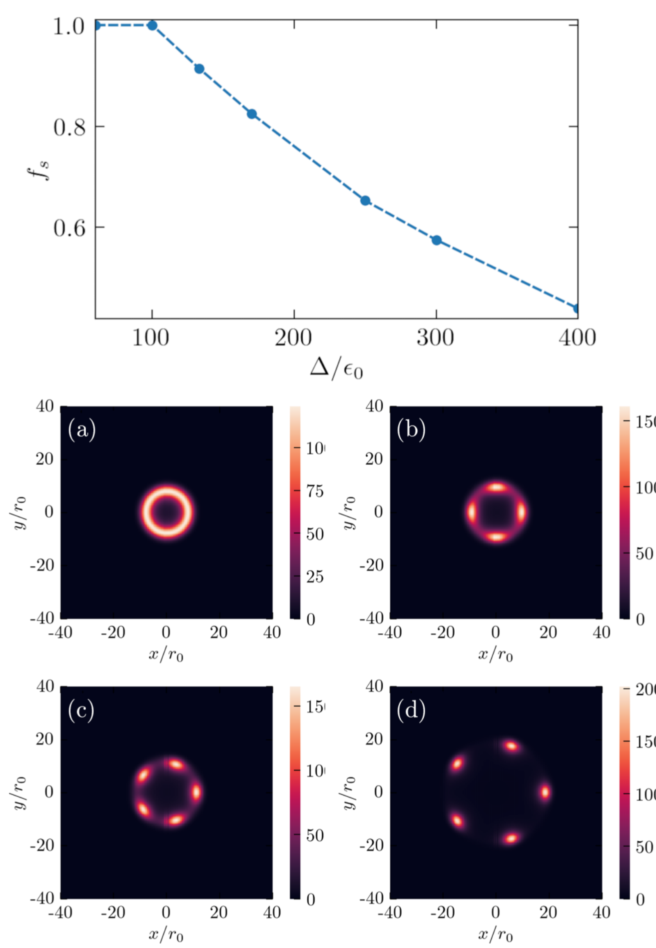

FIG. 6. (Top) Superfluid density as a function of the detuning Δ/ϵ. (Bottom) Integrated density $\rho(x, y)$ for detuning values $\Delta/\epsilon = 100$, 133, 170, and 400 from (a) to (d), respectively. The colorbars indicate the value of $\rho(x, y)$ in units of r_0^{-2}. The ratio between the dipole length and the scattering length is set to $\epsilon_{\rm dd} = 1.38$ and $N = 26500$. The bare harmonic frequency is the same as in Fig. 2.

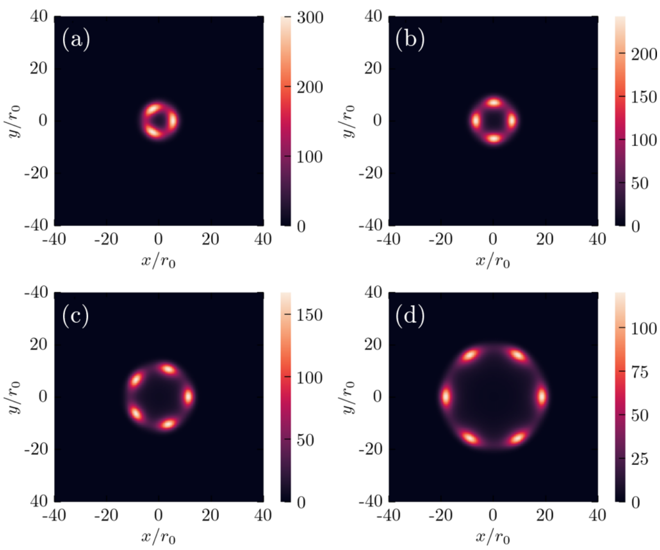

FIG. 7. Ring-shaped supersolid dipolar states are engineered by appropriate combinations of values of the magnetic field detuning, the scattering length and the number of particles. Panels (a)–(d) show the integrated density $\rho(x, y)$ of supersolid states obtained for $\epsilon_{dd} = 1.43$, $N = 26500$, $\Delta/\epsilon = 50$ (a); $\epsilon_{dd} = 1.41$, $N = 26500$, $\Delta/\epsilon = 80$ (b); $\epsilon_{dd} = 1.39$, $N = 26500$, $\Delta/\epsilon = 170$ (c); and $\epsilon_{dd} = 1.37$, $N = 31500$, $\Delta/\epsilon = 400$ (d). The color bars indicate the value of $\rho(x, y)$ in units of r_0^{-2}. The bare harmonic frequency is the same as in Fig. 2.

additional ones, which gets wider as the number of particles increases. Looking at the case with $\varepsilon_{dd} = 1.72$, one can also see that increasing the number of particles leads the system to an unstructured superfluid, meaning that there exists an upper threshold for the particle number above which the solid and supersolid structures disappear. Again, this is in line to the phenomenology reported in the quasi-1D tubular geometry, where in the high-density region of the phase diagram, increasing the density drives a supersolid-to-superfluid phase transition [30,31].

D. Effect of gravity

The structural diagram reported in Fig. 2 has been computed assuming zero gravity conditions. Experimentally, and as stated before, microgravity conditions are achievable in the NASA Cold Atom laboratory in the International Space Station. However, it is interesting to explore the effect of a gravitational force on the dipolar arrangements that have been reported, to study how robust these structures are with respect to gravity. We account for gravitational effects through the inclusion of the one-body potential of Eq. (5). We have performed calculations for $\varepsilon_{dd} = 1.47$, $N = 31500$ (which yields a solid state with three droplets in the absence of gravity) varying the strength of the gravitational field. We first consider a gravity vector with $\theta_g = 0$. The results are shown in Fig. 9. For values of the gravity strength $mg < 0.03mg_E$, the structure of the dipolar BEC is not significantly altered, while for $mg > 0.04mg_E$ we observe the melting of the solid configuration into a superfluid, clusterless state. It is worth noting, though, that close to the value $mg = 0.03mg_E$ the superfluid background present at the bottom of the trap [see Figs. 9(a) and 9(d)] increases the value of Leggett's upper bound for the superfluid fraction, which for the case shown in the figure equals $f_s = 0.43$, while the corresponding simulation in absence of gravity yields $f_s \sim 10^{-2}$. Therefore, for small gravitational fields, a superfluid background is formed at the bottom, providing quantum coherence between droplets. Our results indicate that, for these parameters, the gravitational force field of the Earth would destroy the solid arrangement of droplets, in contrast to what happens in the different parameter regime considered in Ref. [48]. This is because our calculations do not lie in the thin-shell limit considered in Ref. [48], since a tighter trap confinement implies a higher energy cost for particles to accumulate in a reduced space at the bottom of the trap. We have also performed calculations changing the relative orientation between the gravity field and the z axis to $\theta_g = \pi/4$. We show the results in Fig. 10. In this case, we find that the three droplet structure remains unaltered up to $mg \simeq 0.0025mg_E$, where gravity induces a transition into a two droplet state. Further increasing the gravitational strength leads to the merging of the two dipolar clusters into one.

E. Comparison with previous studies

Previous studies have explored the formation of supersolid structures in curved trapping geometries. Authors of Ref. [48] also explore the supersolid properties on dipolar BECs confined in a bubbled trap. However, they do so through the use of an *ab initio* Monte Carlo method. In comparison to the results from Fig. 2, their results involve a considerably lower number of particles ($N < 300$), a shell of smaller radius, and lie in the thin-shell limit, where Eq. (2) is no longer valid, and a pseudopotential that accounts for the curvature of the confinement has to be applied. Reference [48] shows supersolid and solid structures with four dipolar clusters along the equator of the sphere, much like the structure that emerges in region 4 of the structural diagram of Fig. 2. Because of the thin-shell condition, the effect of gravity in the supersolid four droplet structure of Ref. [48] is considerably lower compared to our case, where the more loose trap facilitates the accumulation of particles at the bottom. The physics of dipolar BECs under a bubble trap has also been studied in Ref. [54]. In comparison with our paper, they employ a higher number of particles ($N = 60000$), a considerably higher trap radius $R = 21$ μm and a detuning not equal to the Rabi coupling, $\Delta \neq \Omega$, which favors the emergence of a higher number of dipolar clusters compared to the structures reported in our Fig. 2. Remarkably, it is reported that supersolidity can be induced in solid arrangements of dipolar clusters by inducing a rotation in the system [54]. Other studies have considered different kind of curved geometries, like toroidal traps [50,63] and box traps [68].

Toroidal traps produce ring-shaped supersolids analogous to the ones found in this paper, the difference being that under a shell-shaped confinement, and under microgravity conditions, the ring shape of the supersolid arises naturally from an interplay between the anisotropy of the DDI an the shell shape of the trap, instead of being entirely forced by the ring shape of the toroidal confinement. In Ref. [63], the transition between a fluid ring into a supersolid, with eight dipolar droplets as ε_{dd} increases, is reported. The authors employ a toroidal trap with

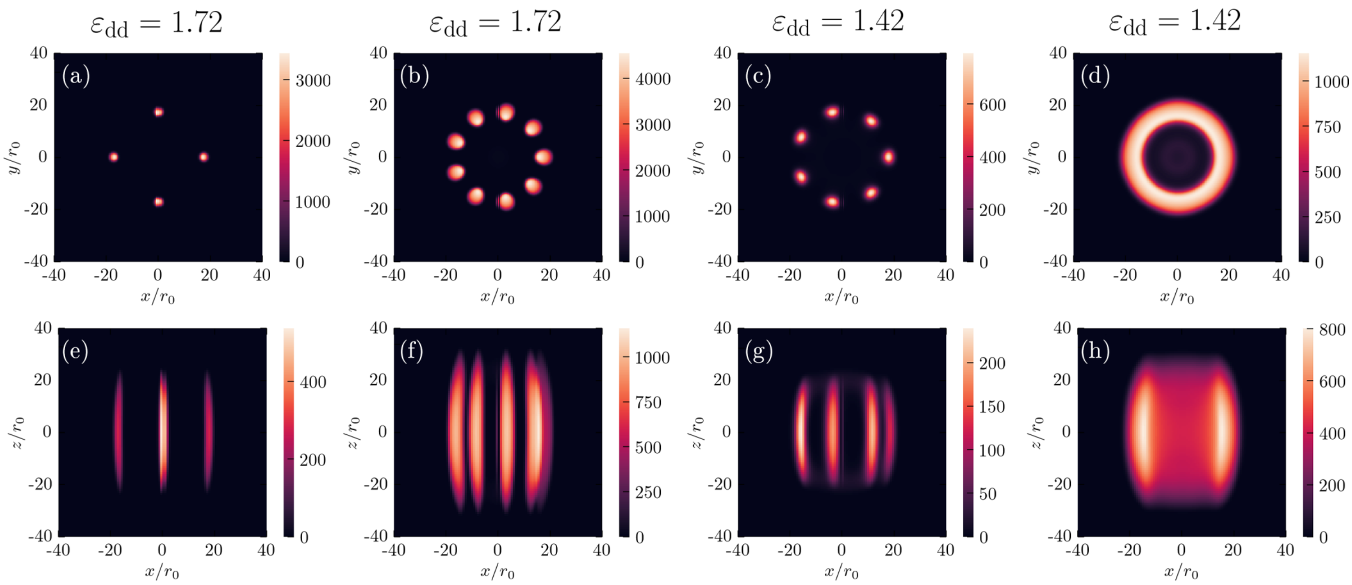

FIG. 8. Integrated densities $\rho(x, y)$ (top) and $\rho(x, z)$ (bottom) for $\varepsilon_{dd} = 1.72, N = 10^5$ [(a), (e)], $\varepsilon_{dd} = 1.72, N = 10^6$ [(b), (f)], $\varepsilon_{dd} = 1.42, N = 10^5$ [(c), (g)], and $\varepsilon_{dd} = 1.42, N = 10^6$ [(d), (h)]. The bubble trap parameters are the same as in Fig. 2. The color bars indicate the value of $\rho(x, y)$ and $\rho(x, z)$ in units of r_0^{-2}.

a considerably higher trapping strength of $\omega = 2\pi \times 1000$ Hz compared to our parameters, which explains the higher number of clusters that they observe compared to our results, since a higher trapping confinement limits the length of the droplets along the polarization direction an hence forces the system to organize in a higher number of clusters. The authors observe a continuous transition between the eight droplet supersolid state and a fully superfluid ring, similarly to the results shown in our Fig. 5 for a supersolid of six droplets. A recent paper has considered the influence of toroidal traps in anti-dipolar BECs [53], where the formation of stacks of ring-shaped droplets, which can coherently overlap to form a supersolid, has been reported. Because of the reversed sign of the DDI, the interaction energetically favors side-by-side arrangements instead of

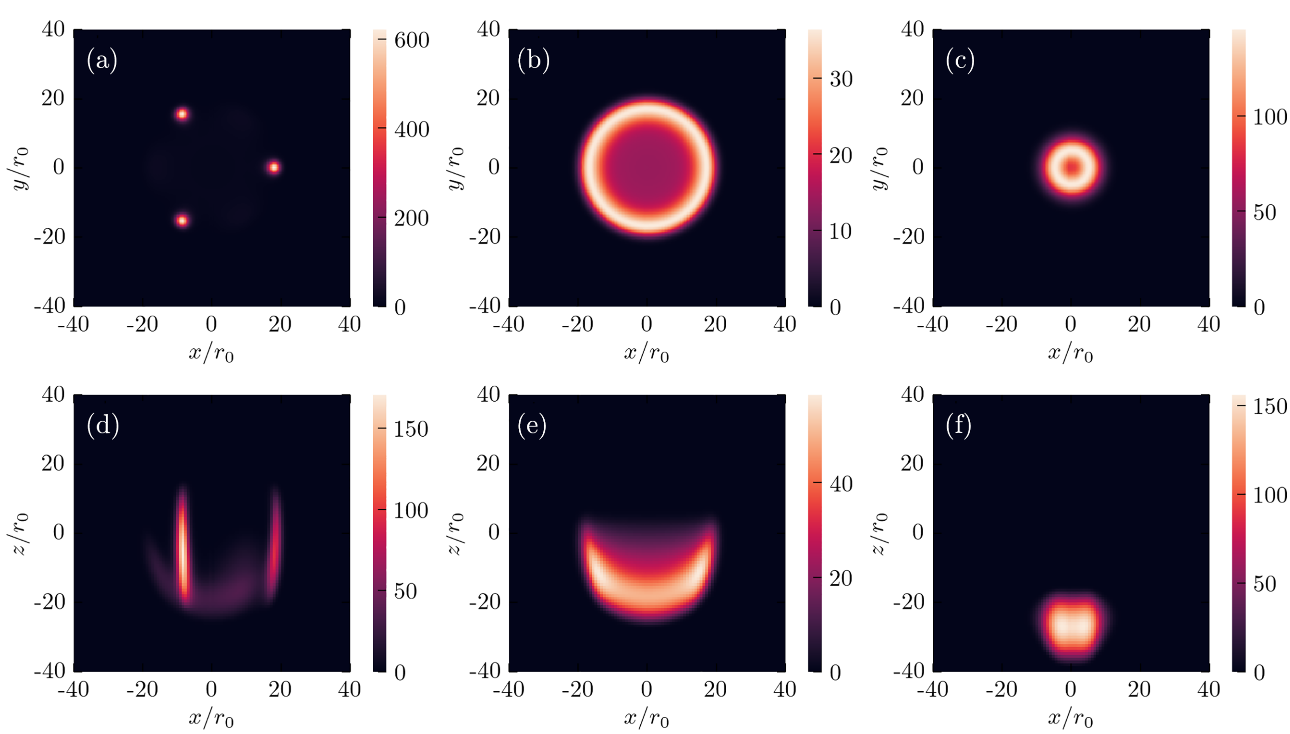

FIG. 9. Integrated densities $\rho(x, y)$ [(a), (c)] and $\rho(x, z)$ [(d)–(f)] for a varying gravitational strength $mg = 0.03mg_E$ [(a), (d)], $mg = 0.04mg_E$ [(b), (e)], and $mg = 0.5mg_E$ [(c), (f)] and an angle $\theta_g = 0$ [see Eq. (5)]. The bubble trap parameters are the same as in Fig. 2. The color bars indicate the value of $\rho(x, y)$ and $\rho(x, z)$ in units of r_0^{-2}.

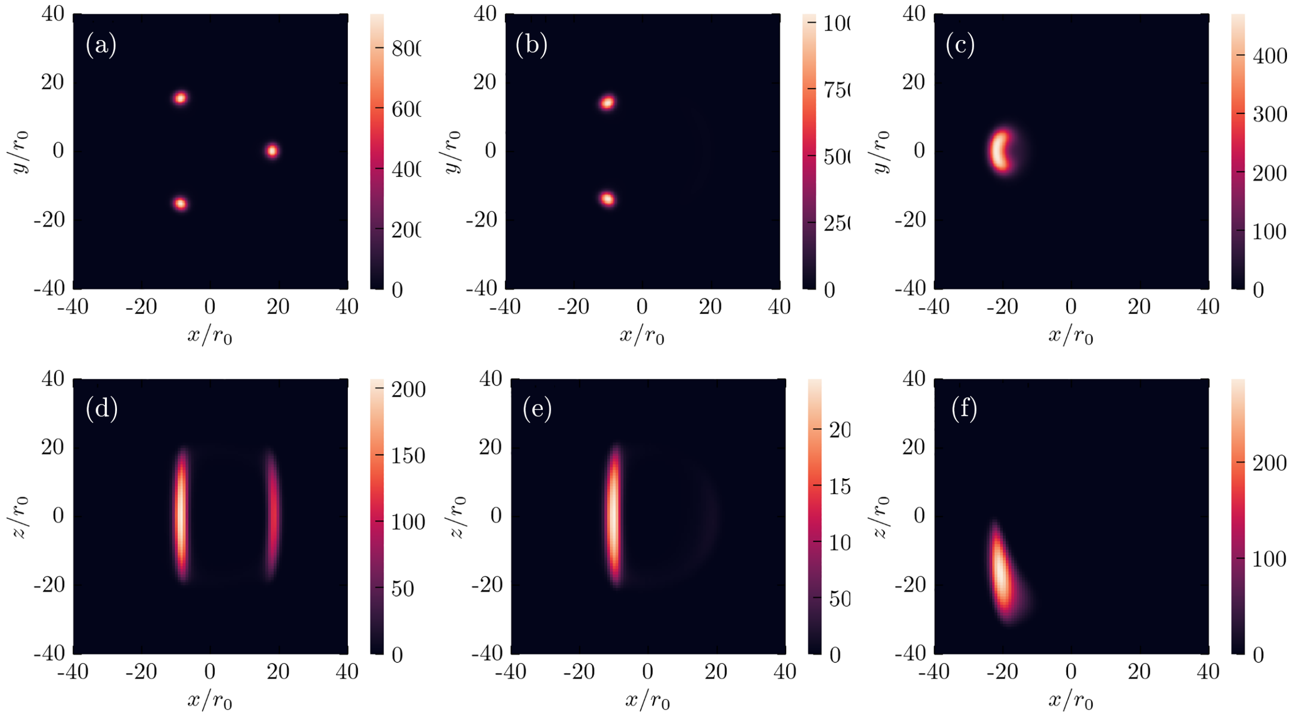

FIG. 10. Integrated densities $\rho(x, y)$ [(a)–(c)] and $\rho(x, z)$ [(d)–(f)] for a varying gravitational strength $mg = 0.0001mg_{\mathrm{E}}$ [(a), (d)], $mg = 0.0025mg_{\mathrm{E}}$ [(b), (e)], and $mg = 0.5mg_{\mathrm{E}}$ [(c), (f)] and an angle $\theta_g = \pi/4$ [see Eq. (5)]. The bubble trap parameters are the same as in Fig. 2. The color bars indicate the value of $\rho(x, y)$ and $\rho(x, z)$ in units of r_0^{-2}.

head-to-tail ones, giving rise to multiple rings placed along the polarization vector of the dipoles, which are relatively thin in this direction, that repel each other. In contrast, in our case, the standard DDI gives rise to arrangements of droplets that are elongated in the polarization direction and distributed along a plane perpendicular to the polarization axis.

In regards to results in a box potential, Ref. [68] explores different shapes for the box confinement, including a cylindrically shaped box trap, where ring solids and supersolids arise. For this kind of confinement, the box-shaped potential allows for the presence of a superfluid bulk in the center of the trap, while supersolid arrangements of droplets are formed in the edges, which allows for the possibility to study interaction effects at the interface of the two phases. In contrast, in our shell-shaped confinement, this superfluid bulk is absent. A similar effect could be induced, however, by applying a small gravitational field, which creates a superfluid background at the bottom of the trap, as shown in in Figs. 9(a)–9(d). In regards to the droplet arrangements observed at the borders of the trap, the authors in Ref. [68] consider a larger number of atoms, which induces the emergence of a larger number of droplets.

IV. CONCLUSIONS

We have studied the interplay between the anisotropy of the dipole-dipole interaction and the curved geometry of the trapping potential for a dipolar condensate confined in a bubble trap. We have provided the structural diagram of a dipolar BEC as a function of the number of particles N and the ratio between the dipole length and the scattering length $\varepsilon_{\mathrm{dd}}$, and have reported the emergence of a wide variety of ring-shaped solid structures formed by arrangements of dipolar clusters along the equator of the trapping potential. We have characterized the transitions between different structures, showing that they are discontinuous, reminiscent of a first-order phase transition in the thermodynamic limit. This establishes a clear connection between our system and a dipolar BEC trapped in a quasi-1D configuration, where, in the low-density regime, a first-order phase transition between a superfluid and a solid phase takes place. We have also explored the high particle number limit ($N > 10^5$) and have observed that atoms accumulate in the central ring along the equator of the trap instead of forming secondary ring-like structures. We have shown that supersolid states with varying number of dipolar clusters can be engineered by changing N, ϵ_{dd}, and the effective radius of the trap, which is accomplished by tuning the detuning of the coupled rf field. In regards to the robustness of the dipolar structures, we have also considered the effect of a gravitational field and have shown that, for our parameters of choice, the gravitational field of the Earth would destroy an arrangement of dipolar droplets, forcing particles to accumulate at the bottom of the trap. Our results lead to the existence of ring-shaped dipolar supersolid states with varying number of clusters which, unlike in the case of ring-shaped traps, are not entirely forced by the confinement geometry, and arise instead as a result of an interplay between the anisotropy of the DDI and the shell-shaped geometry of the bubble trap.

The study of the excitations of these ring supersolids remains a relevant question to be addressed, since it could lead to an experimental protocol to probe the gas-to-supersolid transition by means of measuring excitation frequencies. Also, it remains an open question how finite temperature could affect the physics of the dipolar system under these trapping

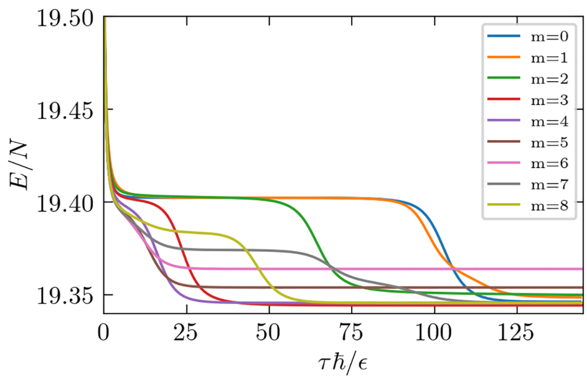

FIG. 11. Energy per particle as a function of the imaginary time for the different initial conditions given by Eq. (A1). The parameters are $\varepsilon_{\mathrm{dd}} = 1.47$, $N = 31500$, $\Delta/\epsilon = 400$.

conditions. Recent results [32,73,74] reveal an important impact of thermal fluctuations on dipolar gases, leading to the counterintuitive formation of a supersolid by heating in the ultracold regime.

ACKNOWLEDGMENTS

We acknowledge financial support from Ministerio de Ciencia e Innovación MCIN/AEI/10.13039/501100011033 (Spain) under Grant No. PID2020-113565GB-C21 and from AGAUR-Generalitat de Catalunya Grant No. 2021-SGR-01411. J.S.-B. and R.B. acknowledge European Union-NextGenerationEU, Ministry of Universities and Recovery, Transformation and Resilience Plan, through a call from the Technical University of Catalonia. R.B. acknowledges funding from ADAGIO (Advanced Manufacturing Research Fellowship Programme in the Basque – New Aquitaine Region) from the European Union's Horizon 2020 Research and Innovation Programme under the Marie Sklodowska Curie cofund Grant Agreement No. 101034379.

APPENDIX: NUMERICAL IMPLEMENTATION

All the results shown in this paper are obtained by propagating Eq. (2) in imaginary time. To do so, we discretize space and work with a grid of $(N_x, N_y, N_z) = (200, 200, 100)$ points, in a simulation box of size $(L_x/r_0, L_y/r_0, L_z/r_0) = (80, 80, 80)$. During imaginary time propagation, we employ a time step of $d\tau\hbar/\epsilon = 0.0005$. The DDI term of Eq. (2) is evaluated by computing its Fourier transform through an FFT routine. As mentioned in the main text, during the imaginary time evolution of Eq. (2) it is very likely for the system to get stuck in a metastable state. Because of this, we run multiple calculations starting from a variety of initial conditions when computing the ground state of the system for a given set of values $(N, \varepsilon_{\mathrm{dd}})$, Δ/ϵ. The set of initial conditions employed is given by

$$\Psi_0(\mathbf{r}) = \exp\left(-\frac{\omega_0\hbar}{\epsilon}(r/r_0 - \sqrt{\Delta/\epsilon})^2\right)(1 + 0.5\cos(m\phi)) \tag{A1}$$

where $r = |\mathbf{r}|$, ϕ is the azimuthal angle and $m = 0, 1, 2, \ldots, 8$. This allows us to start from initial configurations close in shape to those with m number of clusters. After imaginary time evolution, we retain the state with the lowest energy as the ground state. In order to illustrate this process, and to showcase the rich metastable landscape of the system, we show in Fig. 11 the energy as a function of the imaginary time for the different initial states for $\varepsilon_{\mathrm{dd}} = 1.47$, $N = 31500$, $\Delta/\epsilon = 400$.

[1] B. M. Garraway and H. Perrin, Recent developments in trapping and manipulation of atoms with adiabatic potentials, J. Phys. B: At., Mol. Opt. Phys. **49**, 172001 (2016).

[2] D. Becker, M. D. Lachmann, S. T. Seidel, H. Ahlers, A. N. Dinkelaker, J. Grosse, O. Hellmig, H. Müntinga, V. Schkolnik, T. Wendrich *et al.*, Space-borne Bose–Einstein condensation for precision interferometry, Nature (London) **562**, 391 (2018).

[3] Y. Guo, E. M. Gutierrez, D. Rey, T. Badr, A. Perrin, L. Longchambon, V. S. Bagnato, H. Perrin, and R. Dubessy, Expansion of a quantum gas in a shell trap, New J. Phys. **24**, 093040 (2022).

[4] R. A. Carollo, D. C. Aveline, B. Rhyno, S. Vishveshwara, C. Lannert, J. D. Murphree, E. R. Elliott, J. R. Williams, R. J. Thompson, and N. Lundblad, Observation of ultracold atomic bubbles in orbital microgravity, Nature (London) **606**, 281 (2022).

[5] A. Tononi and L. Salasnich, Shell-shaped atomic gases, Phys. Rep. **1072**, 1 (2024).

[6] N. S. Móller, F. E. A. dos Santos, V. S. Bagnato, and A. Pelster, Bose–Einstein condensation on curved manifolds, New J. Phys. **22**, 063059 (2020).

[7] A. Tononi, F. Cinti, and L. Salasnich, Quantum bubbles in microgravity, Phys. Rev. Lett. **125**, 010402 (2020).

[8] A. Tononi and L. Salasnich, Bose-Einstein condensation on the surface of a sphere, Phys. Rev. Lett. **123**, 160403 (2019).

[9] A. Tononi, A. Pelster, and L. Salasnich, Topological superfluid transition in bubble-trapped condensates, Phys. Rev. Res. **4**, 013122 (2022).

[10] Y. He, H. Guo, and C.-C. Chien, BCS-BEC crossover of atomic Fermi superfluid in a spherical bubble trap, Phys. Rev. A **105**, 033324 (2022).

[11] A. Tononi, G. Astrakharchik, and D. S. Petrov, Gas-to-soliton transition of attractive bosons on a spherical surface, AVS Quantum Sci. **6**, 023201 (2024).

[12] A. Tononi and L. Salasnich, Low-dimensional quantum gases in curved geometries, Nat. Rev. Phys. **5**, 398 (2023).

[13] P. Boegel, A. Wolf, M. Meister, and M. A. Efremov, Controlled expansion of shell-shaped Bose–Einstein condensates, Quantum Sci. Technol. **8**, 034001 (2023).

[14] L. Amico, D. Anderson, M. Boshier, J.-P. Brantut, L.-C. Kwek, A. Minguzzi, and W. von Klitzing, *Colloquium:* Atomtronic

circuits: From many-body physics to quantum technologies, Rev. Mod. Phys. **94**, 041001 (2022).

[15] L. Chomaz, I. Ferrier-Barbut, F. Ferlaino, B. Laburthe-Tolra, B. L. Lev, and T. Pfau, Dipolar physics: a review of experiments with magnetic quantum gases, Rep. Prog. Phys. **86**, 026401 (2023).

[16] A. F Andreev and I. M. Lifshitz, Quantum theory of defects in crystals, Sov. Phys. Usp **13**, 670 (1971).

[17] G. V. Chester, Speculations on Bose-Einstein condensation and quantum crystals, Phys. Rev. A **2**, 256 (1970).

[18] A. J. Leggett, Can a solid be "superfluid"? Phys. Rev. Lett. **25**, 1543 (1970).

[19] F. Böttcher, J.-N. Schmidt, J. Hertkorn, K. S. H. Ng, S. D. Graham, M. Guo, T. Langen, and T. Pfau, New states of matter with fine-tuned interactions: quantum droplets and dipolar supersolids, Rep. Prog. Phys. **84**, 012403 (2021).

[20] T. Ilg and H. P. Büchler, Ground-state stability and excitation spectrum of a one-dimensional dipolar supersolid, Phys. Rev. A **107**, 013314 (2023).

[21] J. Hertkorn, J.-N. Schmidt, M. Guo, F. Böttcher, K. S. H. Ng, S. D. Graham, P. Uerlings, T. Langen, M. Zwierlein, and T. Pfau, Pattern formation in quantum ferrofluids: From supersolids to superglasses, Phys. Rev. Res. **3**, 033125 (2021).

[22] A. Gallemí and L. Santos, Superfluid properties of a honeycomb dipolar supersolid, Phys. Rev. A **106**, 063301 (2022).

[23] J. Hertkorn, J.-N. Schmidt, M. Guo, F. Böttcher, K. S. H. Ng, S. D. Graham, P. Uerlings, H. P. Büchler, T. Langen, M. Zwierlein, and T. Pfau, Supersolidity in two-dimensional trapped dipolar droplet arrays, Phys. Rev. Lett. **127**, 155301 (2021).

[24] P. B. Blakie, D Baillie, and S. Pal, Variational theory for the ground state and collective excitations of an elongated dipolar condensate, Commun. Theor. Phys. **72**, 085501 (2020).

[25] R. Bombín, J. Boronat, and F. Mazzanti, Dipolar Bose supersolid stripes, Phys. Rev. Lett. **119**, 250402 (2017).

[26] R. Bombín, F. Mazzanti, and J. Boronat, Berezinskii-Kosterlitz-Thouless transition in two-dimensional dipolar stripes, Phys. Rev. A **100**, 063614 (2019).

[27] Y.-C. Zhang, F. Maucher, and T. Pohl, Supersolidity around a critical point in dipolar Bose-Einstein condensates, Phys. Rev. Lett. **123**, 015301 (2019).

[28] Y.-C. Zhang, T. Pohl, and F. Maucher, Phases of supersolids in confined dipolar Bose-Einstein condensates, Phys. Rev. A **104**, 013310 (2021).

[29] Y.-C. Zhang, T. Pohl, and F. Maucher, Metastable patterns in one- and two-component dipolar Bose-Einstein condensates, Phys. Rev. Res. **6**, 023023 (2024).

[30] P. B. Blakie, D. Baillie, L. Chomaz, and F. Ferlaino, Supersolidity in an elongated dipolar condensate, Phys. Rev. Res. **2**, 043318 (2020).

[31] J. C. Smith, D. Baillie, and P. B. Blakie, Supersolidity and crystallization of a dipolar Bose gas in an infinite tube, Phys. Rev. A **107**, 033301 (2023).

[32] J. Sánchez-Baena, C. Politi, F. Maucher, F. Ferlaino, and T. Pohl, Heating a dipolar quantum fluid into a solid, Nat. Commun. **14**, 1868 (2023).

[33] M. Guo, F. Böttcher, J. Hertkorn, J.-N. Schmidt, M. Wenzel, H. P. Büchler, T. Langen, and T. Pfau, The low-energy Goldstone mode in a trapped dipolar supersolid, Nature (London) **574**, 386 (2019).

[34] L. Tanzi, S. M. Roccuzzo, E. Lucioni, F. Famà, A. Fioretti, C. Gabbanini, G. Modugno, A. Recati, and S. Stringari, Supersolid symmetry breaking from compressional oscillations in a dipolar quantum gas, Nature (London) **574**, 382 (2019).

[35] G. Natale, R. M. W. van Bijnen, A. Patscheider, D. Petter, M. J. Mark, L. Chomaz, and F. Ferlaino, Excitation spectrum of a trapped dipolar supersolid and its experimental evidence, Phys. Rev. Lett. **123**, 050402 (2019).

[36] L. Tanzi, J. G. Maloberti, G. Biagioni, A. Fioretti, C. Gabbanini, and G. Modugno, Evidence of superfluidity in a dipolar supersolid from nonclassical rotational inertia, Science **371**, 1162 (2021).

[37] D. Petter, A. Patscheider, G. Natale, M. J. Mark, M. A. Baranov, R. van Bijnen, S. M. Roccuzzo, A. Recati, B. Blakie, D. Baillie, L. Chomaz, and F. Ferlaino, Bragg scattering of an ultracold dipolar gas across the phase transition from Bose-Einstein condensate to supersolid in the free-particle regime, Phys. Rev. A **104**, L011302 (2021).

[38] G. Biagioni, N. Antolini, A. Alaña, M. Modugno, A. Fioretti, C. Gabbanini, L. Tanzi, and G. Modugno, Dimensional crossover in the superfluid-supersolid quantum phase transition, Phys. Rev. X **12**, 021019 (2022).

[39] T. Bland, E. Poli, C. Politi, L. Klaus, M. A. Norcia, F. Ferlaino, L. Santos, and R. N. Bisset, Two-dimensional supersolid formation in dipolar condensates, Phys. Rev. Lett. **128**, 195302 (2022).

[40] M. A. Norcia, E. Poli, C. Politi, L. Klaus, T. Bland, M. J. Mark, L. Santos, R. N. Bisset, and F. Ferlaino, Can angular oscillations probe superfluidity in dipolar supersolids? Phys. Rev. Lett. **129**, 040403 (2022).

[41] L. Tanzi, E. Lucioni, F. Famà, J. Catani, A. Fioretti, C. Gabbanini, R. N. Bisset, L. Santos, and G. Modugno, Observation of a dipolar quantum gas with metastable supersolid properties, Phys. Rev. Lett. **122**, 130405 (2019).

[42] F. Böttcher, J.-N. Schmidt, M. Wenzel, J. Hertkorn, M. Guo, T. Langen, and T. Pfau, Transient supersolid properties in an array of dipolar quantum droplets, Phys. Rev. X **9**, 011051 (2019).

[43] L. Chomaz, D. Petter, P. Ilzhöfer, G. Natale, A. Trautmann, C. Politi, G. Durastante, R. M. W. van Bijnen, A. Patscheider, M. Sohmen, M. J. Mark, and F. Ferlaino, Long-lived and transient supersolid behaviors in dipolar quantum gases, Phys. Rev. X **9**, 021012 (2019).

[44] M. A. Norcia, C. Politi, L. Klaus, E. Poli, M. Sohmen, M. J. Mark, R. N. Bisset, L. Santos, and F. Ferlaino, Two-dimensional supersolidity in a dipolar quantum gas, Nature (London) **596**, 357 (2021).

[45] A. Filinov, N. V. Prokof'ev, and M. Bonitz, Berezinskii-Kosterlitz-Thouless transition in two-dimensional dipole systems, Phys. Rev. Lett. **105**, 070401 (2010).

[46] M. Ota and S. Stringari, Second sound in a two-dimensional Bose gas: From the weakly to the strongly interacting regime, Phys. Rev. A **97**, 033604 (2018).

[47] P. C. Diniz, E. A. B. Oliveira, A. R. P. Lima, and E. A. L. Henn, Ground state and collective excitations of a dipolar Bose-Einstein condensate in a bubble trap, Sci. Rep. **10**, 4831 (2020).

[48] M. Ciardi, F. Cinti, G. Pellicane, and S. Prestipino, Supersolid phases of bosonic particles in a bubble trap, Phys. Rev. Lett. **132**, 026001 (2024).

[49] M. Arazo, R. Mayol, and M. Guilleumas, Shell-shaped condensates with gravitational sag: contact and dipolar interactions, New J. Phys. **23**, 113040 (2021).
[50] M. Nilsson Tengstrand, P. Stürmer, J. Ribbing, and S. M. Reimann, Toroidal dipolar supersolid with a rotating weak link, Phys. Rev. A **107**, 063316 (2023).
[51] L. E. Young-S. and S. K. Adhikari, Spontaneous dipolar Bose-Einstein condensation on the surface of a cylinder, Phys. Rev. A **108**, 053323 (2023).
[52] M. Šindik, T. Zawiślak, A. Recati, and S. Stringari, Sound, superfluidity and layer compressibility in a ring dipolar supersolid, Phys. Rev. Lett. **132**, 146001 (2024).
[53] K. Mukherjee, T. A. Cardinale, and S. M. Reimann, Selective rotation and attractive persistent currents in anti-dipolar ring supersolids, arXiv:2402.19126.
[54] H. S. Ghosh, S. Halder, S. Das, and S. Majumder, Induced supersolidity and hypersonic flow of a dipolar Bose-Einstein condensate in a rotating bubble trap, arXiv:2402.13422.
[55] Y. Colombe, E. Knyazchyan, O. Morizot, B. Mercier, V. Lorent, and H. Perrin, Ultracold atoms confined in rf-induced two-dimensional trapping potentials, Europhys. Lett. **67**, 593 (2004).
[56] K. Sun, K. Padavić, F. Yang, S. Vishveshwara, and C. Lannert, Static and dynamic properties of shell-shaped condensates, Phys. Rev. A **98**, 013609 (2018).
[57] R. SChützhold, M. Uhlmann, Y. Xu, and U. R. Fischer, Mean-field expansion in Bose–Einstein condensates with finite-range interactions, Int. J. Mod. Phys. B **20**, 3555 (2006).
[58] A. R. P. Lima and A. Pelster, Quantum fluctuations in dipolar Bose gases, Phys. Rev. A **84**, 041604(R) (2011).
[59] A. R. P. Lima and A. Pelster, Beyond mean-field low-lying excitations of dipolar Bose gases, Phys. Rev. A **86**, 063609 (2012).
[60] A. Tononi, Scattering theory and equation of state of a spherical two-dimensional Bose gas, Phys. Rev. A **105**, 023324 (2022).
[61] J. Zhang and T.-L. Ho, Potential scattering on a spherical surface, J. Phys. B: At., Mol. Opt. Phys. **51**, 115301 (2018).
[62] J. Javanainen, S. M. Paik, and S. M. Yoo, Persistent currents in a toroidal trap, Phys. Rev. A **58**, 580 (1998).
[63] M. N. Tengstrand, D. Boholm, R. Sachdeva, J. Bengtsson, and S. M. Reimann, Persistent currents in toroidal dipolar supersolids, Phys. Rev. A **103**, 013313 (2021).
[64] X.-F. Zhang, L. Wen, L.-X. Wang, G.-P. Chen, R.-B. Tan, and H. Saito, Spin-orbit-coupled Bose gases with nonlocal Rydberg interactions held under a toroidal trap, Phys. Rev. A **105**, 033306 (2022).
[65] A. Ramanathan, K. C. Wright, S. R. Muniz, M. Zelan, W. T. Hill, C. J. Lobb, K. Helmerson, W. D. Phillips, and G. K. Campbell, Superflow in a toroidal Bose-Einstein condensate: An atom circuit with a tunable weak link, Phys. Rev. Lett. **106**, 130401 (2011).
[66] K. C. Wright, R. B. Blakestad, C. J. Lobb, W. D. Phillips, and G. K. Campbell, Driving phase slips in a superfluid atom circuit with a rotating weak link, Phys. Rev. Lett. **110**, 025302 (2013).
[67] K. C. Wright, R. B. Blakestad, C. J. Lobb, W. D. Phillips, and G. K. Campbell, Threshold for creating excitations in a stirred superfluid ring, Phys. Rev. A **88**, 063633 (2013).
[68] S. M. Roccuzzo, S. Stringari, and A. Recati, Supersolid edge and bulk phases of a dipolar quantum gas in a box, Phys. Rev. Res. **4**, 013086 (2022).
[69] D. Baillie and P. B. Blakie, Droplet crystal ground states of a dipolar Bose gas, Phys. Rev. Lett. **121**, 195301 (2018).
[70] S. M. Roccuzzo, A. Gallemí, A. Recati, and S. Stringari, Rotating a supersolid dipolar gas, Phys. Rev. Lett. **124**, 045702 (2020).
[71] A. J. Leggett, On the superfluid fraction of an arbitrary many-body system at $T = 0$, J. Stat. Phys. **93**, 927 (1998).
[72] H. Kadau, M. Schmitt, M. Wenzel, C. Wink, T. Maier, I. Ferrier-Barbut, and T. Pfau, Observing the Rosensweig instability of a quantum ferrofluid, Nature (London) **530**, 194 (2016).
[73] M. Sohmen, C. Politi, L. Klaus, L. Chomaz, M. J. Mark, M. A. Norcia, and F. Ferlaino, Birth, life, and death of a dipolar supersolid, Phys. Rev. Lett. **126**, 233401 (2021).
[74] J. Sánchez-Baena, T. Pohl, and F. Maucher, Superfluid-supersolid phase transition of elongated dipolar Bose-Einstein condensates at finite temperatures, Phys. Rev. Res. **6**, 023183 (2024).